






## Collisional shift and broadening of Rydberg states in nitric oxide at room temperature

Fabian Munkes <sup>1</sup>, Alexander Trachtmann,<sup>1</sup> Patrick Kaspar,<sup>1</sup> Florian Anschütz,<sup>1</sup> Philipp Hengel <sup>2</sup>, Yannick Schellander <sup>3</sup>, Patrick Schalberger,<sup>3</sup> Norbert Fruehauf <sup>3</sup>, Jens Anders,<sup>2</sup> Robert Löw,<sup>1</sup> Tilman Pfau,<sup>1</sup> and Harald Kübler <sup>1,\*</sup>

<sup>1</sup>University of Stuttgart, 5th Institute of Physics, Pfaffenwaldring 57, 70569 Stuttgart, Germany

<sup>2</sup>University of Stuttgart, Institute of Smart Sensors, Pfaffenwaldring 47, 70569 Stuttgart, Germany

<sup>3</sup>University of Stuttgart, Institute for Large Area Microelectronics, Allmandring 3b, 70569 Stuttgart, Germany



(Received 31 October 2023; accepted 23 January 2024; published 15 March 2024)

We report on the collisional shift and line broadening of Rydberg states in nitric oxide (NO) with increasing density of a background gas at room temperature. As a background gas we either use NO itself or nitrogen (N<sub>2</sub>). The precision spectroscopy is achieved by a sub-Doppler three-photon excitation scheme with a subsequent readout of the Rydberg states realized by the amplification of a current generated by free charges due to collisions. The shift shows a dependence on the rotational quantum state of the ionic core and no dependence on the principle quantum number of the orbiting Rydberg electron. The experiment was performed in the context of developing a trace-gas sensor for breath-gas analysis in a medical application.

DOI: [10.1103/PhysRevA.109.032809](https://doi.org/10.1103/PhysRevA.109.032809)

### I. INTRODUCTION

By the end of the 1980s it was known that NO plays an important role in the mammalian system [1–3]. In 1998, F. Murad, R. F. Furchgott, and L. J. Ignarro were awarded the Nobel Prize in Physiology or Medicine by The Nobel Foundation for their discoveries concerning NO as a signaling molecule in the cardiovascular system, which ultimately paved the way to a broad field of research [4], involving results on different forms of cancer [5–8] and the role of NO in immunological responses such as inflammation [9]. That NO is also part of the exhaled breath, was shown in 1991 by Gustafsson *et al.* [10], and subsequent research revealed a change in the NO concentration when diseases like asthma, atopy and others are present [11]. The NO concentration in the exhaled breath is in the low-ppb regime, and a guideline [11] suggests that a sensor for breath-gas analysis must be calibrated with samples in the range of 10 to 100 ppb. Such a requirement is challenging when considering, that low gas volumes are preferred. For example, recommendations on the measurement of exhaled NO by the American Thoracic Society (ATS) and the European Respiratory Society (ERS) [11] state, that a patient has to exhale for 10 s at a constant flow to gain about 300 ml of air volume for sensors readily available. In the context of medical research such volumes are expected to be way lower.

We demonstrated a proof-of-concept experiment for a sensor based on the Rydberg excitation of NO (see Ref. [12]), capable of detecting NO concentrations less than 10 ppm limited by preparation, and yet operable at ambient pressure. The extrapolated sensitivity already reached the 10 ppb range. In that experiment, only pulsed laser systems were used. In the experiment presented in this work only continuous-wave

(cw) laser systems are used for the excitation of NO. This ensures selective detection due to the linewidth of cw systems. Our goal in this work is to learn about consequences for the sensor application. As such, we investigate collisional shifts and broadening of the Rydberg line with increasing density of the background gas. This allows us to compare our results with previous results on the pressure broadening and shift in alkalis [13–15]. In a wider context, the consequential improvement in sensitivity may enable us to detect Rydberg bimolecules of NO in the future, which have been predicted theoretically [16].

### II. METHODS

*Setup.* A sketch of the main components of the experimental setup is shown in Fig. 1. All measurements are performed at room temperature,  $T \approx 293$  K. The detection of Rydberg states in NO is realized by the electronic detection of free charges. Therefore, the central part of our setup is a custom designed glass cell with built-in readout electronics.

The cell's glass frame has a copper plate glued to the bottom, whereas the top holds a printed-circuit board (PCB) with an electrode pointing towards the cell's interior and amplification electronics on the other side. Pictures are shown in Fig. 2. Gas may flow through the cell as flange connectors are to the left and right of the frame. Applying a (possibly small) potential to the bottom and top electrodes collects free charges within the cell, and the needed amplification and conversion to a voltage of the current is achieved by the use of a transimpedance amplifier (TIA) with an overall feedback resistance of 1 GΩ. The electrodes have an area of about 472 mm<sup>2</sup>. While a constant and homogeneous field between the electrodes is desirable, a large area of the upper electrode connected to the TIA's input results in a large antenna collecting noise from surrounding sources. Thus, a trade-off has to be made between the two. Our solution is to divide the electrode up into sections, which we all keep at the same potential.

\*h.kuebler@physik.uni-stuttgart.de

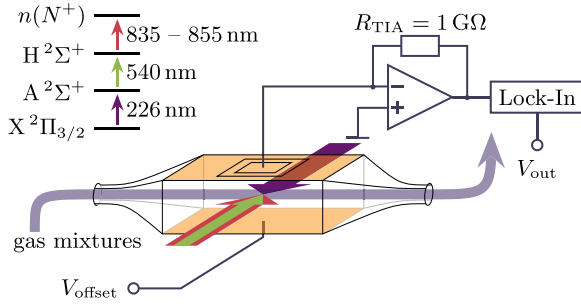


FIG. 1. Sketch of the setup and measurement principle used throughout this work. Gas mixtures of a certain concentration of NO diluted in  $N_2$ , or pure NO, enter the measurement cell on the left. Excitation of NO to a Rydberg state is achieved by a cw three-laser excitation scheme shown in the upper left. Subsequent collisions ionize these molecules. Charges are collected via electrodes, and the current is amplified and converted to a voltage by employing a transimpedance amplifier (TIA). A lock-in amplifier referenced on the modulated second transition improves the signal-to-noise ratio. The cell’s cuboid has a width of 35 mm, a depth of 13.5 mm, and a height of 8.4 mm. Pictures are shown in Fig. 2.

This is indicated in Fig. 1 on the top electrode. In our setup, the outermost part is a solder-resist free ground plane, then an actively driven guard ring follows, and the innermost area centered above the excitation volume is connected to the TIA. This area has dimensions of 13.5 mm  $\times$  10 mm, where the longer side is parallel to the laser beams.

Pressure stability is achieved by using mass-flow controllers (MFC) between the gas bottles and the experimental cell. Two MFCs are used for the experiment, one allows regulating the flow of NO in the range of 0.1 to 5 sccm, and the other regulates the (optional) flow of  $N_2$  in a range of 106 to 100 sccm. If only pure NO is used, the other MFC is closed off by valves. The pressure is constantly monitored at both ends of the cell by pressure gauges.

The NO molecules are excited to a Rydberg state by a three-photon excitation scheme solely by cw laser systems shown in the top left of Fig. 1. We only operate on transitions, where the vibrational quantum  $v$  is  $v = 0$ . While the ultraviolet (UV) beam enters the cell in the

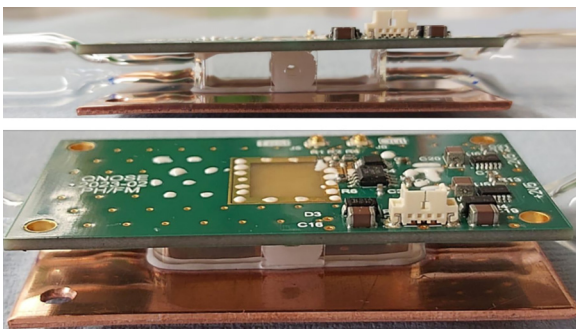


FIG. 2. Pictures of the readout cell. In the center of the upper photo we can see the quartz windows, which are glued to the glass frame, such that the UV light may pass through. On the left and right are the attachments to the MFCs and pumps. The lower photo shows the PCB with readout electronics on top, as well as a copper plate on the bottom, which realizes the counterelectrode.

rear, the two other lasers are counterpropagating, entering from the front. Subsequent collisions of the excited NO molecules with other particles yield free charges, which are electronically detected. The UV system, a frequency-quadrupled titanium-sapphire laser (Ti:Sa), was already introduced in our previous work [17] and is used to drive the first transition,  $A^2\Sigma^+ \leftarrow X^2\Pi_{3/2}$ . The  $1/e^2$  beam waist  $w$  is about 940  $\mu\text{m}$ , and the mean intensity  $I = P/\pi w^2$  is on average 1.8  $\text{mW mm}^{-2}$ . The cw light for the second transition,  $H^2\Sigma^+ \leftarrow A^2\Sigma^+$ , is generated by a 1080-nm diode laser, which is fiber amplified and finally frequency doubled via a single-pass periodically poled lithium niobate crystal. The beam has a waist of about 640  $\mu\text{m}$  and an intensity of on average 480  $\text{mW mm}^{-2}$ . The light for the Rydberg transition  $n(N^+) \leftarrow H^2\Sigma^+$  is another Ti:Sa with a beam waist of 1220  $\mu\text{m}$  used at an intensity ranging from 47  $\text{mW mm}^{-2}$  to 66  $\text{mW mm}^{-2}$ . Note that all beam waist measurements are the average value of values gathered 10 cm in front and after the cell. The intensities are measured directly before entering the cell.

Our setup consists of a separate stabilization setup based on a reference laser at 780 nm locked to an ultralow expansion cavity and then used to stabilize the length of transfer cavities. This allows us to lock the fundamental beams of our excitation lasers to their respective transfer cavities. The Rydberg laser is not locked but scanned during the experiment, and its locked transfer cavity serves as a relative frequency reference. The whole stabilization setup is based on several Red Pitaya STEMLab 125-14A and a self-written lock software built on top of PYRPL [18]. A thorough walkthrough is given in Ref. [19]. Additionally, all fundamental beams are sent to a wavemeter (HighFinesse WS-6) for monitoring.

An improvement in the signal-to-noise ratio is gained by using a lock-in amplifier referenced by the modulation frequency of the second transition. Modulation of the second transition itself is achieved by an acousto-optic modulator, which is driven by the amplified signal of a Red Pitaya STEMLab 125-14A.

*Experimental procedure.* After evacuating the cell by using a backing pump and a turbo pump to about  $1 \times 10^{-5}$  mbar, a constant flow of gas and thus a constant pressure are ensured by the MFCs. Two measurement types are performed, either using pure NO or with mixtures of NO and  $N_2$ . As soon as a stable pressure is achieved, the lasers for  $A^2\Sigma^+ \leftarrow X^2\Pi_{3/2}$  and  $H^2\Sigma^+ \leftarrow A^2\Sigma^+$  are locked to their respective branches. For the UV transition this is the  $P_{12}(6.5)$  branch at roughly 226.982 nm, and for the intermediate transition, the  $R_{11}(5.5)$  branch at about 540.494 nm is used. The wavelengths given are the wavemeter’s readout, which has an inaccuracy of 600 MHz. The initial value of the UV transition was at first simulated with PGOPHER [20] by using constants from Ref. [21]. The initial wavelength of the branch  $R_{11}(5.5)$  of the second transition was taken from Ref. [22].

Finding the two lower and subsequently locked transitions is achieved by scanning and electronically reading out the signal as well. Here, we use higher pressures, about 1 mbar, and higher fields, about 10  $\text{V cm}^{-1}$ . As soon as both transitions are locked the pressure is set a little lower to about 60  $\mu\text{bar}$  and the applied field is reduced to about  $-0.8 \text{ V cm}^{-1}$  to ease finding the Rydberg signal, since this avoids significant broadening and splitting. The Rydberg signal is obtained by scanning the

Ti:Sa operating on  $n(N^+) \leftarrow H^2\Sigma^+$ . Throughout the whole measurement we scan the Rydberg laser and trigger the scope on its ramp. Finally, the pressure is set via the MFC to the desired start pressure. Due to the positions of the gauges, the pressure inside the cell cannot be known exactly. However, a bypass of the cell allows setting inbound and outbound pressure close to each other. Thus, we assume the pressure inside the cell to be the mean of both measured values.

For our measurements we are able to choose the principal quantum number  $n$  as well as the rotational quantum number of the ionic core  $N^+$  of Rydberg states in NO. A state is denoted by  $n(N^+)$ , and we omit specifying the ionic part  $X^+ \Sigma^+$ , as it remains the same. When a state is selected and all starting conditions are met, the experimental data is acquired automatically. Broken down into steps, the procedure is as follows.

(i) Set the applied field to  $E_{\text{field}} \approx -11.9 \text{ V cm}^{-1}$ , which results in a clear distinct splitting of the states due to the Stark effect.

(ii) Adjust the measured frequency range such that the high- $l$  manifolds of the Stark effect are clearly visible. Here we take special care to make the dominant center peak of the manifold visible, which is the one targeted for the evaluation.

(iii) Wait for 45 s to allow the flow (or pressure, respectively) to settle.

(iv) During the scan, the lock-in amplifiers output, the transmission signal of the transfer cavity of the Rydberg laser, and, for checking, the trigger are recorded.

(v) When the scan is complete the flow is changed to the next value.

(vi) Steps (iii) to (v) are repeated.

The measurement series has to be aborted if the reference cavity of the Rydberg laser goes out of lock, since we do not have an absolute frequency reference at hand. Everything is acquired in a “single shot”; i.e., there is no averaging involved. Additionally, we made sure to never reach the electronic limits, i.e., keeping the scan velocity of the Rydberg laser such that it never outperforms the rise time of the electronic circuit and adjusting the lock-in amplifier’s time constant accordingly. In a single shot, we scanned over 13 GHz in 19.9 s, which goes along with a lock-in time constant of 30 ms and a filter order of 3. The rise time of the electronic circuit is below 200  $\mu\text{s}$  and as such negligible.

### III. RESULTS

For the evaluation of our measurements we start by calculating the frequency axis out of the time axis by using the known free-spectral range of the Rydberg laser’s transfer cavity. The peak distances are fitted against the position in time by using a third-order polynomial function. The voltage signal is smoothed by a filter such that a following data reduction is not affecting the quality. Note that the TIA converts and amplifies from current to voltage, and the signal we process here is the lock-in amplifier’s output signal. For each trace the most dominant center peak of the high- $l$  manifold, i.e., the peak not affected by the Stark effect, and the left and right of it are fitted using individual Voigt functions of the form

$$f(\omega) = Af_{\text{Voigt}}(\omega, \omega_0, \gamma_L, \sigma) + \mathcal{P}_3(\omega), \quad (1)$$

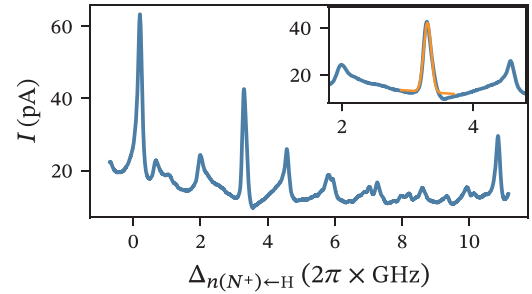


FIG. 3. Exemplary measurement trace of a pure NO measurement of 32(4) at a density of  $N_{\text{NO}} \approx 1.91(57) \times 10^{15} \text{ cm}^{-3}$ . The inset shows the fit of the nonmoving centered line, which is used to obtain the relevant data. The fit aligns well with the overall shape of the peak and is as such sufficient to extract both the FWHM and its frequency position.

where  $\mathcal{P}_3(\omega)$  is a polynomial function of third order to account for the baseline,  $A$  is the amplitude,  $\gamma_L$  is the Lorentzian part of the full width at half maximum (FWHM),  $\gamma_G = 2\sqrt{2 \log(2)}\sigma$  is the Gaussian part of the FWHM, and  $\omega_0$  is the center position relevant to extract the shift. The Voigt function  $f_{\text{Voigt}}$  is normalized to its amplitude. Special care is taken for the polynomial bounds such that the effects on the parameters of interest are negligible. While we only look at the center peak, the side peaks are fitted for consistency checking. In Fig. 3 we show an exemplary measurement trace including a fit.

We use

$$\gamma \approx \frac{1}{2} \left[ 1.0692 \frac{\gamma_L}{2} + \sqrt{0.86639 \left( \frac{\gamma_L}{2} \right)^2 + 4\gamma_G^2} \right] \quad (2)$$

from Ref. [23] to calculate the overall FWHM  $\gamma$ . Note that we would expect a Lorentzian shape due to the homogeneity of collisional broadening. However, as we will see later, additional contributions such as the small pressure shift of the second transition  $H^2\Sigma^+ \leftarrow A^2\Sigma^+$  are present in our experiment. During the evaluation we verified that a fit with a Voigt function suits our results best. In Fig. 4 we show our results for the FWHM  $\gamma$  and the relative shift  $\delta$ .

We start by considering the pressure broadening of the selected Rydberg state  $n(N^+)$ . In general, several mechanisms contribute to the broadening of the linewidth  $\gamma$  of the Rydberg line, namely, residual Doppler broadening, power broadening, transit-time broadening, and broadening due to polarization effects. In the case of NO it is hard to give numbers to Doppler broadening, power broadening, or polarization effects as literature values were inconsistent [24–26]. However, in the case of Doppler broadening, a lower bound can be given by taking the linewidth of  $2\pi \times 15 \text{ MHz}$  as seen in Ref. [17] of the UV transition and accounting for the  $k$ -vector mismatch, which yields around  $2\pi \times 8 \text{ MHz}$ . Additionally, the linear behavior shown in Fig. 4 suggests that collisional effects are dominating. In the case of collisions of NO with NO or NO with  $\text{N}_2$ , the broadening is basically the same with increasing density of the perturber.  $\text{N}_2$  and NO differ only by a single electron when considering the orbital structure. For NO only one of the two levels of the  $\pi_{2p}^*$  is occupied with a single electron [27], whereas for  $\text{N}_2$  all are empty. This makes the broadening contributions similar. The Boltzmann distribution, describing

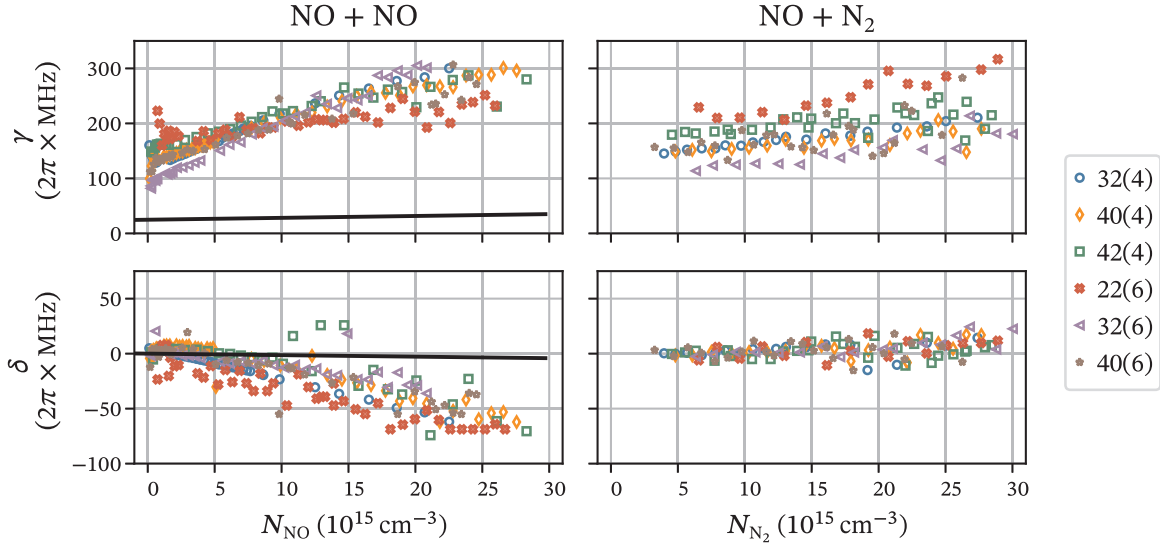


FIG. 4. FWHM  $\gamma$  and relative shift  $\delta$  for NO being subject to an increasing density  $N$  of the background gas, either NO itself on the left or  $N_2$  on the right. Plotted are the results for different principal quantum numbers  $n$  and rotational quantum numbers  $N^+$  of the ionic core [Hund's case (d)], and the notation  $n(N^+)$  is used in the legend. The relative shift is moved such that the first measurement points are referenced to zero. The solid line indicates possible contributions by effects on the  $H^2\Sigma^+$  state as explained in the text. For the measurements of NO perturbed by  $N_2$  the NO density was  $0.6(3) \times 10^{15} \text{ cm}^{-3}$ .

the population of the rotational levels for a diatomic molecule, is given by Herzberg as [28]

$$P(J) = hcB_v \frac{2J+1}{k_B T} \exp\left[-hc \frac{B_v J(J+1)}{k_B T}\right], \quad (3)$$

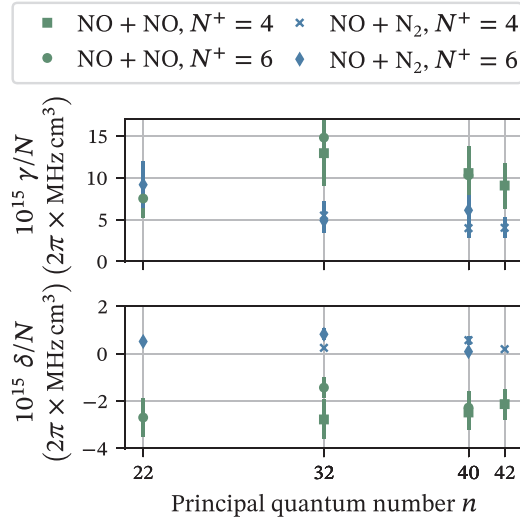


FIG. 5. Broadening rate  $\gamma/N$  and shift rate  $\delta/N$  of the perturbation of Rydberg states in NO. We explain the high broadening rate in comparison to alkalis as seen in Refs. [14,15] by the additional degrees of freedom in a molecule. Some exemplary alkali values are given in Table I. An uncertainty of 30% in the measured pressure is indicated by error bars. For some measurement points the marker covers the error bar. Within the error the values are constant, which is expected when compared to alkalis. The individual values are given in Table II.

where  $P(J)$  is the population probability of having a rotational state with the total angular momentum  $J$  at temperature  $T$  occupied. The Planck constant is denoted by  $h$ ,  $k_B$  is the Boltzmann constant, and  $c$  is the speed of light. For NO, the rotational constant  $B_v$ , as given in Ref. [21], yields that rotational levels from  $J = 0.5$  to  $J = 19.5$  have a population probability above 1%, suggesting significant contribution to the broadening. At a later point we will compare our results to measurements done in alkalis. It is worth noting that any alkali, being a simple atom, lacks these additional contributions [14,15].

Consider the relative shift  $\delta$  next. Based on Fermi's work [13], elastic collisions between the Rydberg electron and perturbing atoms or molecules lead to the frequency shift  $\delta$  of

$$\delta = 2\pi \frac{\hbar}{m_e} aN, \quad (4)$$

where  $N$  denotes the density,  $m_e$  is the electronic mass,  $a$  is the scattering length, and  $\hbar$  is the reduced Planck constant. In the case of NO perturbed by NO, a red shift can be seen. In the case of perturbations by  $N_2$ , the considered density range indicates a slight shift to the blue less than the scattering of the measured values for the different states  $n(N^+)$ . Inelastic collisions do not lead to a phase shift in the Rydberg electron's wave function but change the state of the Rydberg atom or molecule itself. While both collision types may occur, this gives an indication of likeliness. For a rare gas, such elastic collisions are expected due to the closed-shell structure [14,15]. Interestingly our results show similar results for perturbations of NO with NO itself. A possible explanation for this is that NO has a degenerate level in the  $\pi_{2p}^*$  available, suggesting that elastic collisions may occur despite the rotational and vibrational freedom. This explanation is supported by the fact that the molecule  $\text{NO}^-$ , though short-lived, even exists



TABLE I. Selected exemplary values at different principal quantum numbers  $n$  of Rydberg states in alkalis from measurements taken by Weber and Niemax [15] and Füchtbauer *et al.* [14]. For measurements by Füchtbauer *et al.*, Rydberg states of potassium (K) are perturbed by argon (Ar), and for measurements by Weber and Niemax, we take their values of rubidium (Rb) Rydberg  $nS$  states perturbed by argon. In the case of Füchtbauer *et al.*, we calculated the rates by using the ideal gas law.

| $n$ | Füchtbauer <i>et al.</i> [14]                            | Weber and Niemax [15]                                    |  |
|-----|--|--|--|
|     | K + Ar   | (nS) Rb + Ar   |  |
|     | $\delta/N$<br>( $10^{-15} 2\pi \times \text{MHz cm}^3$ ) | $\gamma/N$<br>( $10^{-15} 2\pi \times \text{MHz cm}^3$ ) | $\delta/N$<br>( $10^{-15} 2\pi \times \text{MHz cm}^3$ ) |
| 21  | -10.97   | 1.46   | -4.76  |
| 23  | -10.94   | 1.56   | -4.94  |
| 25  | -11.34   | 1.66   | -5.02  |
| 27  |  | 1.77   | -5   |
| 29  |  | 1.8  | -5   |
| 33  |  | 1.36   | -5.16  |
| 35  |  | 1.36   | -5.04  |

in biological processes [29]. However, when looking at  $N_2$ , a similar argument could be made. From our measurements it is undecidable if a particular collision type is dominating for both cases. Our experiment is only sensitive to the effective scattering length, which can be the average of positive and negative scattering lengths for each channel.

We performed similar measurements without the Rydberg laser to investigate the effect on the  $H^2\Sigma^+$  state. This means we locked the lowest transition, scanned the  $H^2\Sigma^+ \leftarrow A^2\Sigma^+$  transition, and read out electronically. Note that the applied field of about  $11.9 \text{ V cm}^{-1}$  is not enough to produce a visible Stark splitting. Hence, the evaluation focused on a single peak, but was done in the same way as for the Rydberg transition otherwise. While a broadening and shift could be observed, its contribution is negligible. We show this in an added solid line to Fig. 4, where we scaled a linear fit to these measurements by the wave-vector mismatch as was done in Eq. (4) in Ref. [30]:

$$\frac{k_1 - k_2 - k_3}{k_1 - k_2} \approx 0.53. \quad (5)$$

The resulting scaled functions are

$$\gamma(N)/2\pi \approx 10^{-15} \text{ MHz cm}^3 \times N + 24.87 \text{ MHz}, \quad (6a)$$

$$\delta(N)/2\pi \approx -10^{-15} \text{ MHz cm}^3 \times N. \quad (6b)$$

While we do not have to consider this contribution for the overall behavior, the contribution by the intermediate transition  $H^2\Sigma^+ \leftarrow A^2\Sigma^+$  partly explains the necessity of using a Voigt function for fitting rather than a Lorentzian. Further inhomogeneities might arise from the already introduced available degrees of freedom in a molecule.

In a next step we compare our results with results from the literature. Füchtbauer *et al.* [14] as well as Weber and Niemax [15] both investigated the shift of spectroscopic lines of alkalis being subject to a perturbing rare gas. In Füchtbauer *et al.*'s experiment the alkalis sodium and potassium were subject to collisions with three different rare gases: helium, neon,

TABLE II. Broadening and shift rate,  $\gamma/N$  and  $\delta/N$ , extracted from a fit to the measurement results shown in Fig. 4. The fit functions are explained in the text. The main error contribution to the values is the absolute pressure uncertainty of 30% of the used gauges. A plot of these values is shown in Fig. 5.

| State    | NO + NO  |  | NO + $N_2$   |  |
|----------|--|--|--|--|
|          | $\gamma/N$<br>( $10^{-15} 2\pi \times \text{MHz cm}^3$ ) | $\delta/N$<br>( $10^{-15} 2\pi \times \text{MHz cm}^3$ ) | $\gamma/N$<br>( $10^{-15} 2\pi \times \text{MHz cm}^3$ ) | $\delta/N$<br>( $10^{-15} 2\pi \times \text{MHz cm}^3$ ) |
| $n(N^+)$ |  |  |  |  |
| 32(4)    | 13(4)  | -2.8(8)  | 5.5(16)  | 0.25(8)  |
| 40(4)    | 11(3)  | -2.5(7)  | 4.0(12)  | 0.57(17)   |
| 42(4)    | 9.1(27)  | -2.1(6)  | 4.0(12)  | 0.19(6)  |
| 22(6)    | 7.5(23)  | -2.7(8)  | 9.2(28)  | 0.52(16)   |
| 32(6)    | 15(4)  | -1.4(4)  | 4.9(15)  | 0.82(25)   |
| 40(6)    | 10(3)  | -2.3(7)  | 6.1(18)  | 0.089(27)  |

and argon. In Weber and Niemax's experiment the rubidium  $nD$  and  $nS$  transitions were shifted by helium, xenon, and argon. In contrast to Füchtbauer *et al.*, Weber and Niemax were able to analyze the broadening as well. Comparison is easiest when using the broadening rate  $\gamma/N$  and the shift rate  $\delta/N$  as introduced by Weber and Niemax. In Table I we list some exemplary literature values. We give both values extracted from a fit to the data plotted in Fig. 4 and listed in Table II. The fit of the shift against the density is done by a linear function in accordance with Eq. (4). For the broadening we use

$$f_{\text{fit}}(N) = \sqrt{\text{offset}^2 + \left(\frac{\gamma}{N}N\right)^2} \quad (7)$$

as a fit function to account for additional broadening contributions such as the residual Doppler broadening in the low densities by an offset. We give an error estimate to all fitted values as well. The largest contribution to our errors has its origin in the absolute pressure given by our pressure gauges (Pfeiffer PKR 251) and amounts to 30%. In contrast, as seen in Ref. [17], the uncertainty of our frequency axis,  $2\pi \times 2.5 \text{ MHz}$ , can in this case be neglected. Therefore, the error given is based solely on the pressure uncertainty. In comparison with Refs. [14, 15], our broadening rate  $\gamma/N$  is several times higher than their values. The shift rate  $\delta/N$  deviates at least by a factor of 2, when comparing measurements of NO and alkalis, which indicates that additional processes are present in molecules.

#### IV. SUMMARY

We showed the collisional shift and broadening of Rydberg states in NO with increasing density of two background gases. The detection of the Rydberg states was realized by an electrical readout of the current generated by free charges resulting from collisions. The linear shift of elastic collisions can be understood as introduced by Fermi [13].

The measurement was performed on either NO being perturbed by itself or  $N_2$ . Comparison to literature values [14, 15] of the experiment was achieved by extracting the broadening rate  $\gamma/N$  and the shift rate  $\delta/N$  using fits to our experimental data. The analysis showed that we are unable to determine

in our experiment which collision type is dominating. In any case our rates deviate at least by a factor of 2, when compared to measurements done in alkalis. We attribute this to the additional degrees of freedom in NO.

The overall project's goal is to realize a breath-gas sensor for NO in the context of a possible medical application. Our work shows that the main effect to consider is the broadening rate, since it is larger than the shift rate. This allows for an optimal choice of background densities depending on the excitation bandwidths given by the lasers and other broadening mechanisms present in the system, e.g., power broadening. Another significant step towards the realization is the reduction of the cross-sensitivity to other gases present in the

breath. Here, we could use our current setup, but change the background gas, for example, to CO<sub>2</sub>.

#### ACKNOWLEDGMENTS

This project has received funding from the European Union's Horizon 2020 research and innovation programme under Grant No. 820393 (macQsimal) as well as by the Deutsche Forschungsgemeinschaft (DFG, German Research Foundation) - 431314977/GRK2642. Additionally, we thank Prof. S. Hogan, Dr. M. Rayment, Prof. H. Sadeghpour, and Prof. R. González Férrez for fruitful discussions and valuable advice.

- 
- [1] W. P. Arnold, C. K. Mittal, S. Katsuki, and F. Murad, Nitric oxide activates guanylate cyclase and increases guanosine 3':5'-cyclic monophosphate levels in various tissue preparations, *Proc. Natl. Acad. Sci. USA* **74**, 3203 (1977).
- [2] R. F. Furchgott and J. V. Zawadzki, The obligatory role of endothelial cells in the relaxation of arterial smooth muscle by acetylcholine, *Nature (London)* **288**, 373 (1980).
- [3] L. J. Ignarro, G. M. Buga, K. S. Wood, R. E. Byrns, and G. Chaudhuri, Endothelium-derived relaxing factor produced and released from artery and vein is nitric oxide, *Proc. Natl. Acad. Sci. USA* **84**, 9265 (1987).
- [4] L. J. Ignarro, Nitric oxide is not just blowing in the wind, *Br. J. Pharmacol.* **176**, 131 (2019).
- [5] G. Haklar, E. Sayin-Özveri, M. Yüksel, A. Aktan, and A. Yalçın, Different kinds of reactive oxygen and nitrogen species were detected in colon and breast tumors, *Cancer Lett.* **165**, 219 (2001).
- [6] S. K. Choudhari, G. Sridharan, A. Gadbaill, and V. Poornima, Nitric oxide and oral cancer: A review, *Oral Oncol.* **48**, 475 (2012).
- [7] W. Xu, L. Z. Liu, M. Loizidou, M. Ahmed, and I. G. Charles, The role of nitric oxide in cancer, *Cell Res.* **12**, 311 (2002).
- [8] F. H. Khan, E. Dervan, D. D. Bhattacharyya, J. D. McAuliffe, K. M. Miranda, and S. A. Glynn, The role of nitric oxide in cancer: Master regulator or NOt? *Int. J. Mol. Sci.* **21**, 9393 (2020).
- [9] D. D. Thomas, L. A. Ridnour, J. S. Isenberg, W. Flores-Santana, C. H. Switzer, S. Donzelli, P. Hussain, C. Vecoli, N. Paolucci, S. Ambs, C. A. Colton, C. C. Harris, D. D. Roberts, and D. A. Wink, The chemical biology of nitric oxide: Implications in cellular signaling, *Free Radical Biol. Med.* **45**, 18 (2008).
- [10] L. E. Gustafsson, A. M. Leone, M. G. Persson, N. P. Wiklund, and S. Moncada, Endogenous nitric oxide is present in the exhaled air of rabbits, guinea pigs and humans, *Biochem. Biophys. Res. Commun.* **181**, 852 (1991).
- [11] American Thoracic Society and European Respiratory Society, ATS/ERS recommendations for standardized procedures for the online and offline measurement of exhaled lower respiratory nitric oxide and nasal nitric oxide, *Am. J. Respir. Crit. Care Med.* **171**, 912 (2005).
- [12] J. Schmidt, M. Fiedler, R. Albrecht, D. Djekic, P. Schalberger, H. Baur, R. Löw, N. Fruehauf, T. Pfau, J. Anders, E. R. Grant, and H. Kübler, Proof of concept for an optogalvanic gas sensor for NO based on Rydberg excitations, *Appl. Phys. Lett.* **113**, (2018).
- [13] E. Fermi, Sopra lo spostamento per pressione delle righe elevate delle serie spettrali, *Nuovo Cim.* **11**, 157 (1934).
- [14] C. Füchtbauer, P. Schulz, and A. F. Brandt, Verschiebung von hohen serienlinien des natriums und kaliums durch fremdgase, berechnung der Wirkungsquerschnitte von delgasen gegen sehr langsame elektronen, *Z. Phys.* **90**, 403 (1934).
- [15] K. H. Weber and K. Niemax, Impact broadening and shift of RbnS and nD levels by noble gases, *Z. Phys. A: At. Nucl.* **307**, 13 (1982).
- [16] R. González-Férez, J. Shertzer, and H. Sadeghpour, Ultralong-range Rydberg bimolecules, *Phys. Rev. Lett.* **126**, 043401 (2021).
- [17] P. Kaspar, F. Munkes, P. Neufeld, L. Ebel, Y. Schellander, R. Löw, T. Pfau, and H. Kübler, *Phys. Rev. A* **106**, 062816 (2022).
- [18] L. Neuhaus, R. Metzдорff, S. Chua, T. Jacqmin, T. Briant, A. Heidmann, P.-F. Cohadon, and S. Deléglise, PyRPL (Python Red Pitaya Lockbox)—An open-source software package for FPGA-controlled quantum optics experiments, in *2017 European Conference on Lasers and Electro-Optics and European Quantum Electronics Conference* (Optica Publishing Group, 2017), paper EA\_P\_8.
- [19] M. Mäusezahl, F. Munkes, and R. Löw, Tutorial on locking techniques and the manufacturing of vapor cells for spectroscopy [arXiv:2401.16068](https://arxiv.org/abs/2401.16068).
- [20] C. M. Western, PGOPHER: A program for simulating rotational, vibrational and electronic spectra, *J. Quant. Spectrosc. Radiat. Transfer* **186**, 221 (2017).
- [21] J. Danielak, U. Domin, R. Ke, M. Rytel, and M. Zachwieja, Reinvestigation of the emission  $\gamma$  band system ( $A^2\Sigma^+-X^2\Pi$ ) of the NO molecule, *J. Mol. Spectrosc.* **181**, 394 (1997).
- [22] Y. Ogi, M. Takahashi, K. Tsukiyama, and R. Bersohn, Laser-induced amplified spontaneous emission from the 3d and nf Rydberg states of NO, *Chem. Phys.* **255**, 379 (2000).
- [23] J. J. Olivero and R. L. Longbothum, Empirical fits to the Voigt line width: A brief review, *J. Quant. Spectrosc. Radiat. Transfer* **17**, 233 (1977).
- [24] L. G. Piper and L. M. Cowles, Einstein coefficients and transition moment variation for the NO ( $A^2\Sigma^+-X^2\Pi$ ) transition, *J. Chem. Phys.* **85**, 2419 (1986).

- [25] A. B. Callear and I. W. M. Smith, Fluorescence of nitric oxide. Part 1.—Determination of the mean lifetime of the  $A^2\Sigma^+$  state, *Trans. Faraday Soc.* **59**, 1720 (1963).
- [26] R. de Vivie and S. D. Peyerimhoff, Theoretical spectroscopy of the NO radical. I. Potential curves and lifetimes of excited states, *J. Chem. Phys.* **89**, 3028 (1988).
- [27] M. Schulz-Weiling, Ultracold molecular plasma, Ph. D. thesis, University of British Columbia, Vancouver, CA, 2017, <http://hdl.handle.net/2429/62516>.
- [28] G. Herzberg, *Spectra of Diatomic Molecules*, 2nd ed., Molecular Spectra and Molecular Structure (Van Nostrand, New York, 1950), Vol. 1.
- [29] M. N. Hughes, Relationships between nitric oxide, nitroxyl ion, nitrosonium cation and peroxyxynitrite, *Biochim. Biophys. Acta, Bioenerg.* **1411**, 263 (1999).
- [30] H. Kübler and J. P. Shaffer, A read-out enhancement for microwave electric field sensing with Rydberg atoms, in *Quantum Technologies 2018*, edited by A. J. Shields, J. Stuhler, and M. J. Padgett (SPIE, Bellingham, WA, 2018).